A Note on the Barotropic Response of Sea Level to Time-dependent Wind Forcing

Lee-Lueng Fu and Roger A. Davidson

June, 1995

Jet Propulsion Laboratory

California Institute of Technology

Pasadena, CA 91109

(Submitted to the JGR TOPEX/POSEIDON Special Issue)

Abstract

This study examines the extent to which sea level variations at periods less than a year and spatial scales greater than 1000 km can be described by the wind-driven linear barotropic vorticity dynamics. The TOPEX/POSEIDON altimetric observations of sea level and the wind products of the National Meteorological Center are used as the database for the study. Each term of the linear barotropic vorticity equation was evaluated by averaging over regions of 10° x 10°. In most of the open ocean, the result of the analysis suggests that the sea level variabilities at the scales considered cannot be fully described by the equation; the apparent net vorticity change is more than what can be explained by the local wind stress curl. In the few regions where the wind stress curl is strong enough to balance the vorticity budget, predominantly in the northeast Pacific and the southeast Pacific, the balance is basically achieved in terms of the time-dependent topographic Sverdrup relation -- the balance between the advection of the planetary vorticity plus the topography-induced vorticity and the forcing by the wind stress curl.

Introduction

The response of the ocean to time-varying wind forcing has been a subject of numerous theoretical investigations (e.g., Veronis and Stommel, 1956; Phillips, 1966; Philander, 1978; Willebrand et al., 1980; Muller and Frankingnoul, 1981; Samelson, 1989; Cummins, 1991). The description is often made in terms of the barotropic (depth-independent) and the baroclinic (depth-dependent) modes. It is generally believed that the response of the ocean to wind forcing at mid and high latitudes is primarily barotropic when the scale of the forcing is much larger than 100 km and the period of the forcing is between the inertial period and about 300 days (Willebrand et al, 1980). In the quasi-geostrophic limit, the dynamics of the ocean's response can be described to a large extent by the linear barotropic vorticity equation:

$$\frac{\partial}{\partial t}\nabla^2\eta+\beta\frac{\partial\eta}{\partial x}-\frac{f}{H}\left(\frac{\partial\eta}{\partial x}\frac{\partial H}{\partial y}-\frac{\partial\eta}{\partial y}\frac{\partial H}{\partial x}\right) = \frac{f}{\rho g}(\nabla\times(\tau/H))_z \qquad (1)$$

where η is the sea level, H the ocean depth, τ the wind stress, p the water density, g the local gravitational constant, f= 2 Ω sin (latitude), Ω the Earth's rotation rate, β = df/dy. On the left-hand side of the equation, the first term is the time rate of the change of the relative vorticity, expressed in terms of $\nabla^2\eta$, the second term is the advection of the planetary vorticity, and the third term is the advection of the vorticity induced by the bottom topography. The right-hand side of the equation is the forcing by the wind stress curl. If the wind stress and sea level is known everywhere, this equation can be used to evaluate the barotropic response of the ocean to wind forcing.

A number of terms have been neglected in (l). The ratio of the neglected nonlinear advection of relative vorticity to the advection of planetary vorticity (the second term) is given by a non-dimensional number defined as $U/(\beta L^2)$ (e.g., Rhines, 1977), which is about 1/1000 for the case considered in the present paper. Another neglected term is the vorticity generation by the stretching of the water column, proportional to $(f^2/gH)\, d\eta/dt$, which is about 1/100 of the planetary vorticity term based on a time scale of 10 days.

There is ample observational evidence for directl y wind-forced ocean currents (Koblinsky and Niiler, 1982; Niiler and Koblinsky, 1985; Koblinsky et al. 1989; Brink, 1989; Samelson, 1990; Luther et al., 1990; Chave, 1992; Niiler et al., 1993). Coherence of deep currents with both local and remote wind forcing was documented and explained in terms of the barotropic response of the ocean. However, there has been little observational evidence for a predominantly barotropic response of the ocean to wind forcing in the open ocean at spatial scales on the order of 1000 km and time scales shorter than seasonal, the scales prescribed by Willebrand et al. (1980) for barotropic response. Are the oceanic variabilities at those scales primarily forced by wind according to (1)? In the present study we try to address this question by using the global sea level observations from the radar altimeter aboard the TOPEX/POSEIDON satellite (Fu et al, 1994) to investigate the relationship between the sea level and wind in the context of (1). The wind data are primarily obtained from the National Metrological Center (NMC) model of the atmospheric circulation. The wind data from the ERS-1 scatterometer are also used for comparison.

The Data and Procedures

Several satellite altimeters were flown before TOPEX/POSEIDON; however, none of them had sufficient measurement accuracies for detecting the large-scale weak signals (generally less than 10 cm) in the sea level created by the barotropic ocean currents.

TOPEX/POSEIDON is the first altimetric mission with adequate measurement accuracy to study the large-scale global ocean dynamics. The first 550 days' worth of the mission's data were used in this study. The standard corrections recommended in Callahan (1994) were applied to the altimeter@ including the inverted barometer correction (Fu and Pihos, 1994). Additionally, an empirical tidal corrections (Fu, Pihos, and Zlotnicki, unpublished manuscript, 1994) were applied to reduce the residual tidal errors after the application of the tide model of CartWright and Ray (1990). This empirical correction model is similar to that of Schrama and Ray (1994) with an estimated residual tidal error of 3-4 cm.

The orbit of the satellite repeats its ground track every 9.9156 days (a nominal 10-day repeat period). Along each altimeter ground track, all the repeat measurements were interpolated to a set of common ground points 6.2 km apart. After removing the temporal mean sea level at each point, the sea level residuals were smoothed and subsampled every 5th point along the satellite ground track. The resulting data were mapped globally to lox 1° grids at 5 day intervals.

The mapping was performed using the objective analysis of Bretherton et al. (1976). Centered on each grid point, a space-time window of 600 km and 40 days was used to collect data for estimating the sea level at the grid point. A Gaussian covariance function was used for both the sea level signal and the observation error. The e-folding scale for the sea level signal was 300 km in space and 30 days in time. These scales were chosen to represent a compromise of a wide range of energy-containing scales that varies geographically. The magnitude of the sea level signal assumed by the covariance function for the mapping was 10 cm, a globally representative value. The spatial scale for the observation error was 15(X) km along the satellite track, reflecting the large scales of the dominant errors from the uncertainties in the tides, orbit, and sea-state effects. However, the error is assumed to be uncorrelated from track to track. The magnitude of the observation error for the covariance function is estimated to be about 6 cm (the root-sum-squares of 4.7 cm from altimetry and 3.5 cm from tides; see Fu et al., 1994). The resulting error for the sea level estimate obtained from the objective mapping analysis is about 2 cm with a scale about 1000 km, which was obtained as part of the mapping calculation.

Two additional data products are required to evaluate (l): wind and bathymetry. The wind product of the National Meteorological Center (NMC) model at 1000 mb was converted to wind stress on a 2.5° x 2.5° grid at 12 hour intervals using a drag coefficient based on Liu et al. (1979). The wind stress data were subsequent y smoothed and subsampled at the same 5 day interval as the altimeter data using a 10-day running average. The bathymetry data were obtained from the ETOPO5 global elevation database which is available on a l/12°x 1/12° grid. The data were smoothed by a running averaging box of 2° x 2° to provide a smoothed bathymetry that is affecting the large scale flow of interest. The choice of the smoothing scale is based on the study of Koblinksy et al. (1989), who reported that a smoothing scale of 175 km resulted in the best agreement with the theoretical analysis based on the topographic Sverdrup relation.

It is believed that sea level variations at seasonal and interannual time scales are dominated by the baroclinic motions. To study the barotropic variability which is expected at shorter time scales, both the sea level and wind data are high-pass filtered to retain only the variabilities at scales shorter than seasonal. Because of the relatively short duration of the data records, we simply removed from the data an annual harmonic plus a second-degree polynomial fit to the data instead of using more sophisticated filters. Shown in Figure 1 are the variance-preserving spectra (frequency times power density) of sea level and wind stress curl at a selected site (45° N, 180° E). Plotted this way, the variance is proportional to the area under the spectrum. The focus of the present study is on the energies at the intraseasonal regime from 20 to 100 days.

Since the bulk of the barotropic variability is expected primarily at spatial scales much larger than 100 km, the balance of(1) was evaluated in terms of areal averages performed for each term of(1) over areas of 10°x 10° in size centered on a 5° x 5° grid. At smaller scales the energetic mesoscale eddies would mask the existence of any barotropic variabilities. Due to the concern of tidal errors and other dynamical processes in shallow coastal areas, areas which have depths less than 1000 m were excluded from the analysis. The areal averaging has reduced small-scale variabilities in both the wind and sea level data. The correlation between the the resultant time series of the vorticity and the wind stress curl is used to examine the validity of (l). Based on the Stokes Theorem, the areal integrals of the wind stress curl term and the relative vorticity term of equation (1) were evaluated as contour integrals performed around the perimeter of the area, with the integrand being the along-contour component of the wind stress for the former and the cross-contour component of the horizontal gradient of the sea level for the latter. The planetary vorticity term was evaluated as the meridional integral of the zonal sea level differences across the box. The areal integral of the topography term was performed via summation over finite areal elements. To express the results in unit of the time rate of vorticity change, sec^{-2}, the resultant value for each term of(1) was multiplied by g/f for the following discussions.

An estimate of the error in evaluating each term of (1) based on the procedures described above is made. As noted above the relative vorticity term (the first term) is evaluated as a line integral of the sea level gradient around the perimeter of each averaging box. The error in estimating the term is derived similarly, based on the fact that the mapped sea level has an error of about 2 cm over a scale of 1000 km. With the Coriolis parameter and its north-south gradient evaluated at a latitude of 45 degrees, the resulting error for the relative vorticity term is estimated about 0.5 x10^{-14} see^{-2}, based on a time scale of 10 days (the error decreases with increasing time scale). The error for the planetary vorticity term (the second term), evaluated similarly, is about 3 x 10^{-14} see^{-2}. The regions where significant correlations of vorticity with wind are found are places of relatively mild variability in bottom topography with a slope of 10^{-4} to 10^{-3}. Taking 0.5 x10-3 for the bottom slope, the error for the topographic term is about 2 x 10^{-14} see^{-2}. Assuming a 0.5 dyne error for the wind stress (for a 2 m/s speed error at wind speed of 7 m/s), the error for the wind forcing term is about 1 x 10^{-14} sec^{-2}. As discussed below, these error estimates are comparable to the signals within order of magnitude.

Results

The analysis described above was applied to all the deep oceans on a 5°x 5° grid. At each grid point, a time series was generated for each term of (l). We first compared the magnitude of the forcing (the right-hand side of (1)) to that of the vorticity budget (the left-hand side of(l)). Shown in Figure 2 is the ratio of the rms variability of the forcing to that of the vorticity budget. It is apparent that over most of the open ocean the wind stress curl does not have sufficient energy to balance the vorticity budget at the scales considered. Based on a 30-day decorrelation time scale, the Fisher's F probability distribution (e.g., Jenkins and Watts, 1968) indicates that the rms ratio less than 0.7 is significantly different from unity at 95 % confidence level. However, the estimation error for the vorticity is probably larger than that for the wind stress curl (see the preceding section) by a factor of 2-3, making the significant ratio reduced to about 0.5.

There are only limited regions where the wind forcing has sufficient energy to account for the vorticity variation. The regions within which the ratio is close to unity can only be found in the Northeast Pacific and the mid- and high-latitude South Pacific. These are the regions of large wind stress curl variability resulting from the prevailing atmospheric synoptic-scale storms. Shown in Figure 3 is a map of the rrns variability of the curl of (τ/H), indicating that the latitudinal dependence in Figure 2 is mostly dictated by the pattern of the wind forcing modified by the bottom topography. At lower latitudes, the time scales of large scale baroclinic motions are shorter than their high latitude counterparts, making the barotropic motions less detectable in the scale regime considered. Near the equator (within about 3 degrees in latitude) (1) is obviously inadequate because of the breakdown of the quasi-geostrophic approximation. At mid and high latitudes, the longer time scales of the baroclinic motions and the larger wind stress curl provide favorable conditions for the detection of the relatively fast barotropic response.

Within the regions where the wind forcing and the vorticity budget have comparable magnitudes, the two sides of(1) are approximately balanced if they are positively correlated Also shown in Figure 1 are the regions (20 of them) where there are significant correlations (greater than 0.4 based on a 30 day decorrelation scale and a 90 % confidence level) between the wind forcing and the vorticity, and in the mean time the ratio of the rms wind variability to therms vorticity budget is greater than 0.33 (mostly greater than 0.5). Only in these regions, predominantly in the northeast and southeast Pacific, is (1) in approximate balance. Listed in Table 1 are various statistics associated with (1) for the 20 regions. The magnitudes of the various terms of (1) (the last 4 columns) are evaluated as the rms of the associated time series. Based on comparison to the error estimate discussed in the preceding section, the signal-to-noise ratio for the vorticity estimate is on the order of unity, while the wind stress curl has a slightly higher signal-to-noise ratio. Figures 4 and 5 show the comparisons between the wind forcing and the vorticity budget at selected regions in the North and the South Pacific, respectively. Despite the discrepancies whose magnitudes are consistent with the error estimate, there is a visual correlation, especially at

periods of **30-60 days.** Shown in Figure 6 is the average coherence between the wind stress curl and the vorticity budget for the six selected regions. The coherence is above the 95% confidence level with near-zero phase at most periods longer than 20 days, the Nyquist period for the altimetry observation.

A scale analysis of the individual vorticity terms on the left-hand side of (1) indicates that the first term (the time rate of change) tends to be dominated by the second and/or the third terms, as revealed in Table 1. Therefore the balance of (1) tends to be achieved among the forcing and the advection of the planetary vorticity and/or the topography-induced vorticity, corresponding to the time-dependent topographic Sverdrup balance. Displayed in Figure 7 are the time series of each term of (1) at a couple of selected sites, clearly showing the dominance of the planetary vorticity and the topographic terms in balancing the wind forcing.

The topographic Sverdrup balance is not commonly observed in the ocean. Koblinsky et al. (1989) examined observations from current meters in the deep oceanat31 sites in the North Pacific and found only a few of them showing evidence for the balance. Most of these sites were north of 35° N and within the regions where the present study shows evidence for the balance (Figure 1). Cummins (1991) pointed out that it was difficult to observe the balance using point measurements. Using a barotropic ocean model, he showed that the topographic Sverdrup balance emerged only after the vorticity equation was averaged over periods longer than 40 days and spatial scales larger than about 400 km. Small scale variability generated by bottom topography makes the detection of the topographic Sverdrup balance difficult in the velocity measurements made by individual current meters.

Dushaw et al. (1994) estimated barotropic currents and relative vorticity from a triangular acoustical tomography array (about 1000 km on each side of the triangle) centered around 38° N and 200° E. They found that the wind stress curl (based on the Navy Fleet Numerical Oceanographic Center wind product) was too weak (by an order of magnitude) to achieve the topographic Sverdrup balance. However, the present study shows that the wind stress curl (based on the NMC product) in this region is sufficiently strong to balance the vorticity budget and that the correlation between the two is marginally significant.

At low latitudes where the wind stress curl is weak, it is apparent that the estimation error in evaluating the vorticity budget exceeds the magnitude of the wind foxing. It is thus possible that the apparent failure of (1) is due to the estimation error instead of the failure of the barotropic dynamics. If this is true, namely, (1) is still valid when the wind forcing is weak, then significant correlations ought to be found among the various terms on the left-hand side of (l), indicating the dominance of the homogeneous solutions to (l). The left-hand side of(1) is then dominated by the residuals from imperfect cancellations of large terms. However, this is not the case. We have not found significant correlations among the left-hand side terms in the low latitude regions. The results from Chao and Fu (1995) who examined the simulation by an ocean general circulation model also indicate that significant barotropic motions are primarily located at mid and high latitudes where the forcing by wind stress curl is strong.

The results of the study are also dependent on the quality of the wind stress curl calculated from the NMC winds. Because the focus of the study is on large scales, the errors in the small scales, where the model winds are expected to be poor, do not affect the calculation in a fundamental way. To verify this assumption to some extent, we also carried out the same calculations using the ERS- 1 wind product (provided by Tim Liu and

Wendy Tang of JPL) during the period when it is available. This wind product was based on a first guess field from the ECW (European Center for Medium-Range Weather Forecast) winds, with ERS-1 observation blended in by a successive correction method (Tripoli and Krishnamurti, 1975). The results are fairly similar to the ones based on the NMC winds. A couple of examples are shown in Figure 8 for comparison to Figure 4. Therefore, we feel that the large-scale wind stress curl derived from the NMC winds is not significantly different from the ERS-1 based result.

Concluding Discussions

The results of the present study suggest that in most part of the open ocean, the large-scale, low-frequency sea level variabilities with periods less than 1 year cannot be fully described by the barotropic vorticity equation given by (1). The wind stress curl is typically too weak to balance the vorticity budget. Although the estimation error for the vorticity is not small, it does not appear to dominate the signal. There maybe other dynamic processes at work at the scales examined resulting in sea level variabilities other than those explained by the barotropic response of the ocean to wind forcing. These are probably large-scale baroclinic waves which have relatively short periods at low latitudes (e.g., Le Traon and Minster, 1993; Jacobs et al, 1993). In regions of strong boundary currents such as the Kuroshio, the Gulf Stream, and the Brazil/Malvinas Confluence region, the dynamics of the large-scale variabilities are not well understood. The non-linear interaction of the gyre with its boundary currents may create short-period, gyre-scale sea level variations.

In the few regions where the wind stress curl is strong enough to balance the vorticity budget, predominantly in the northeast Pacific and the southeast Pacific, the balance is basically achieved in terms of the time-dependent topographic Sverdrup relation. The results of the present study in the northeast Pacific are consistent with those of Koblinsky et al. (1989), who reported the existence of the topographic Sverdrup balance from a few deep current meter observations generally located in the same regions where the present study suggests the same balance in the barotropic vorticity equation. Using the SeaSat scatterometer and altimeter data, Mestas-Nunez et al. (1992) showed that the South Pacific was approximately in a time-dependent Sverdrup balance over a 3 month period without invoking the topographic effects. However, the present study suggests that the topographic effects are also important in that region.

Wunsch (1991) applied a multi-channel linear regression model to the Geosat sea level observation and the NMC wind velocity in the North Pacific and North Atlantic. He was able to relate the observed large-scale sea level variability to the wind velocity variability empirically in the two oceans. The present study suggests that the dynamical relationship between sea level and wind is not readily transparent in most of the oceans.

Freely propagating barotropic Rossby waves are homogeneous solutions to (1). It is difficult to detect them in the presence of strong local wind forcing. Gaspar and Wunsch (1989) and Jacobs et al. (1993) reported only marginal detection of free Rossby waves in altimetric sea level observations. However, detection of significant coherence between deep current observations and remote wind forcing has been documental in many investigations (Niiler et al., 1993; Brink, 1989; Samelson, 1990; Luther et al., 1990), indicating the existence of free barotropic Rossby waves. The wavelengths of these waves are generally shorter than 1000 km and not resolvable by the present analysis. The periods for wavelengths longer than 1000 km are generally less than 20 days and hence not resolvable by the sampling scheme of TOPEX/POSEIDON.

Chao and Fu (1995) examined the barotropic stream function of an ocean general circulation model and found strong correlation with the intraseasonal large-scale sea level variability. There are four regions where the sea level variability can be identified with barotropic motions: the central North Pacific north of 35° N, the southeast Pacific, the southeast Indian Ocean southwest of Australia, and the South Atlantic south of 35° S. The present study suggests that part of these variabilities (the northeast Pacific and the southeast Pacific in particular) can be described by the linear barotropic vorticity equation, but the remaining of them seems to require a model with more complicated barotropic dynamics.

Acknowledgements

The research described in the paper was carried out by the Jet Propulsion Laboratory, California Institute of Technology, under contract with National Aeronautics and Space Administration. The work is supported by the TOPEX/POSEIDON Project under an Announcement of Opportunity. The assistance of Akiko Hayashi and Greg Pihos in processing the TOPEX/POSEIDON data, as well as the provision of the ERS- 1 wind products by Wendy Tang and Tim Liu, is acknowledged The authors have benefited ii-em several useful discussions with Peter Niiler.

References

Bretherton, F.P., R. E. Davis, and **C.B.** Fandry, A technique for objective analysis and design of oceanographic experiments applied to MODE-73, Deep-Sea ***Res.,*** 23,559-582, 1976.

Brink, K.H., Evidence for Wind-Driven Current Fluctuations in the Western North Atlantic. ***J. Geophys. Res.,*** 94 ***(C2),*** 2029-2044,1989.

Callahan, P. S., ***Topex/Poseidon Project GDR Users Handbook,*** JPL D-8944 (internal document), rev A, Jet Propulsion Laboratory, Pasadena, Calif., 84 pp., 1994.

Cartwright, D.E. and **R.D.** Ray, Oceanic tides from **Geosat** altimetry, ***J. Geophys. Res.,*** 95,3069-3090, 1990.

Chao, Y., and L.-L. Fu, A comparative study of an **ocean** general circulation model with **TOPEX/POSEIDON** observations, submitted to ***J. Geophys. Res., 1995.***

Chave, A.D., **D.S.** Luther, and **J.H. Filloux,** The **Barotropic Electromagnetic** and Pressure Experiment 1. **Barotropic Current** Response to Atmospheric Forcing. ***J. Geophys. Res.,*** 97 ***(C6),*** 9565-9593, 1992.

Cummins, P.F., The **Barotropic** Response of the SubPolar North Pacific to Stochastic Wind Forcing. ***J. Geophys. Res.,*** 96 ***(C5),*** 8869-8880, 1991.

Dushaw, B.D., P.F. Worcester, and B.D. Cornuelle, Barotropic currents and vorticity in the central North Pacific Ocean during summer 1987 determined from long-range reciprocal acoustic transmissions. *J. Geophys. Res.,* 99 (C2), 3263-3272, 1994.

Fu, L-L., and G. Pihos, Determining the response of sea level to atmospheric pressure forcing using TOPEX/POSEIDON data, *J. Geophys.Res.*, 99,24633-24642, 1994.

Fu, L.-L., E. J. Christensen, C. Yamarone, M. Lefebvre, Y. Menard, M. Dorrer, and P. Escudier, 1994: TOPEX/POSEIDON Mission Overview. *J. Geophys. Res.,* 99,24369-24381, 1994.

Gaspar, P. and C. Wunsch, Estimates from Altimeter Data of Barotropic Rossby Waves in the Northwestern Atlantic Ocean. *J. Phys. Oceanogr,. 19(12),* 1821-1844,1989.

Jacobs, G. A., W.J. Emery and G.H. Born, Rossby waves in the Pacific Ocean extracted from Geosat altimeter data. *J. Phys. Oceanogr., 23,1155-1175,1993.*

Jenkins, G.M., and D.G. Watss, *Spectral Analysis and Its Applications,* Holden-Day, San Francisco, 525 pp., 1968.

Koblinsky, C.J., and P.P. Niiler, The relationship between deep ocean currents and winds east of Barbados, *J. Phys. Oceanogr., 12,* 144-153, 1982.

Koblinsky, C.J., P.P. Niiler and W.J. Schmitz, Jr., Observations of Wind-Forced Deep Ocean Currents in the North Pacific. *J. Geophys. Res.,* 94 *(C8),* 10,773-10,790, 1989.

Le Traon, P.-Y. and J.-F. **Minster,** Sea Level Variability and Semiannual Rossby Waves in the South Atlantic Subtropical **Gyre.** ***J. Geophys. Res., 98(C7), 12315-12326, 1993.***

Liu, W.T., **K.B. Katsaros,** and **J.A. Businger,** Bulk **parameterization** of air-sea exchanges in heat and water vapor including the molecular constraints at the interface ***J. Atmos. Sci.,*** 36, 1722-1735, 1979.

Luther, D. S., **A.D. Chave, J.H. Filloux,** and **P.F.** Spain, Evidence for **Local** and Nonlocal **Barotropic** Responses to Atmospheric **Forcing During Bempex.** ***Geophys. Res. Lett., 17(7),*** 949-952, 1990.

Mestas-Nunez, A.M., **D.B. Chelton** and **R.A. DeSzoeke,** Evidence **of** Time-Dependent **Sverdrup** Circulation in the South Pacific from Seasat **Scatterometer** and Altimeter. ***J. Phys. Oceanogr., 22(8), 934-943, 1992.***

Müller, P. and C. **Frankignoul,** Direct Atmospheric Forcing of **Geostrophic** Eddies. JPO, ***11,*** 287-308, 1981.

Niiler, P.P. and **C.J. Koblinsky,** A Local Time-Dependent **Sverdrup** Balance in the Eastern North Pacific Ocean. ***Science,*** 229,754-756, 1985.

Niiler, P.P., J. **Filloux, W.T.** Liu, **R.M. Samelson, J.D.** Paduan, and **C.A.** Paulson, Wind-Forced Variability of the Deep Eastern North Pacific: Observations of Seafloor Pressure and Abyssal Currents. ***J. Geophys. Res.,*** 98 ***(C12),*** 22,589-22,602, 1993.

Philander, S.G.H., Forced oceanic waves, ***Rev. Geophys. Space Phys., 16, 15-46, 1978.***

Phillips, N. A., Large-scale eddy motion in the western Atlantic, ***J. Geophys. Res., 71***, 3883-3891, 1966.

Samelson, R.M., Evidence for Wind-Driven Current Fluctuations in the Eastern North Atlantic. ***J. Geophys. Res.***, 95 ***(C7)***, 11,359-11,368, 1990.

Schrama, E.J.O., and R.D. Ray, A preliminary tidal analysis of TOPEX/POSEIDON altimetry, ***J. Geophys.Res., 99, this*** issue, 1994.

Tripoli G.J. and T.N. Krishnamurti, Low-level flows over the GATE area during summer 1972, ***Mon Weather Rev, 103, 197-209, 1975.***

Veronis, G., and H. Stommel, The action of variable wind stresses on a stratified ocean, ***J. Mar. Res., 15,43-75, 1956.***

Willibrand, J., S.G.H. Philander, and R.C. Pacanowski, The Oceanic Response to Large-Scale Atmospheric Disturbances. ***J. Phys. Oceanogr., 10,411-429, 1980.***

Wunsch, C., Large-scale response of the ocean to atmospheric forcing at low frequencies, ***J. Geophys. Res,*** 96, 15083-15092, 1991.

Figure Captions

Figure 1. Spectra for the sea level (solid line) and wind stress curl (dashed line) averaged over a 10° x 10° box centered at 45° N and 180° E. The spectra are shown in a varaince-preserving form (frequency times power density) inarbitrary units.

Figure 2. Contours of the ratio of the rms variability of the wind stress curl to the rms variability of the vorticity budget. The contours of 0.4 and 0.8 are shown in lines of medium thickness, whereas the lines of maximum thickness delineate the boundaries within which the analysis was performed. The shaded regions are those where the correlation coefficients between the vorticity budget and the wind stress curl is greater than 0.4 and the ratio of therms vorticity budget to therms wind stress curl is greater than 0.33.

Figure 3. Contours of the rms viability of the curl of (τ/H), the forcing term on the right-hand side of (l). The unit is 10^{-13} see^{-2}.

Figure 4. Time series of the vorticity budget (solid lines) and the wind stress curl (dashed lines) for Regions # 4, 9, 13, and 14 in the North Pacific. Refer to Table 1 for more information.

Figure 5. Same as Figure 2 except for Regions# 5 and 17 in the South Pacific. Refer to Table 1 for more information.

Figure 6. Average coherence between the vorticity and the wind stress curl at the 6 sites shwon in Figures 4-5. The amplitude is shown at the top and the phase at the bottom. The dashed line represents the 95 % confidence level for non-zero coherence.

Figure 7. The various terms of (l): the time rate of relative vorticity (dotted), the planetary vorticity (short dashed), the topography-induced vorticity (long dashed), and the wind forcing (solid). (A) at 30 N, 220 E (region # 13). (B) at 45 N, 220 E (region # 14)

Figure 8. Same as Figure 4 except that the wind stress is based on the ERS-1 observations for Regions # 13 and 14. Compare to Figure 4.

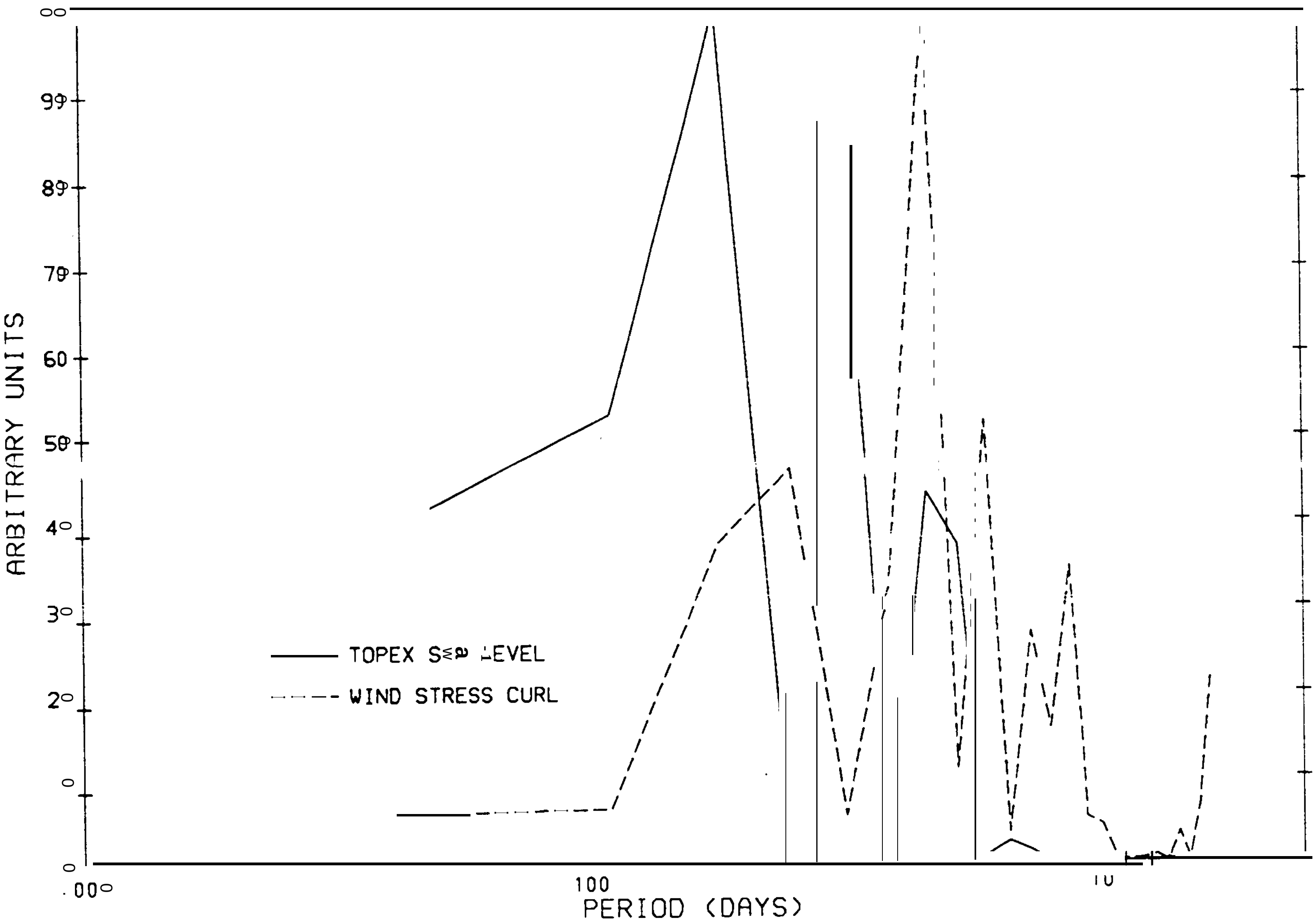
ARBITRARY UNITS
PERIOD (DAYS)
100
10
TOPEX Sea LEVEL
WIND STRESS CURL

Fig. 1

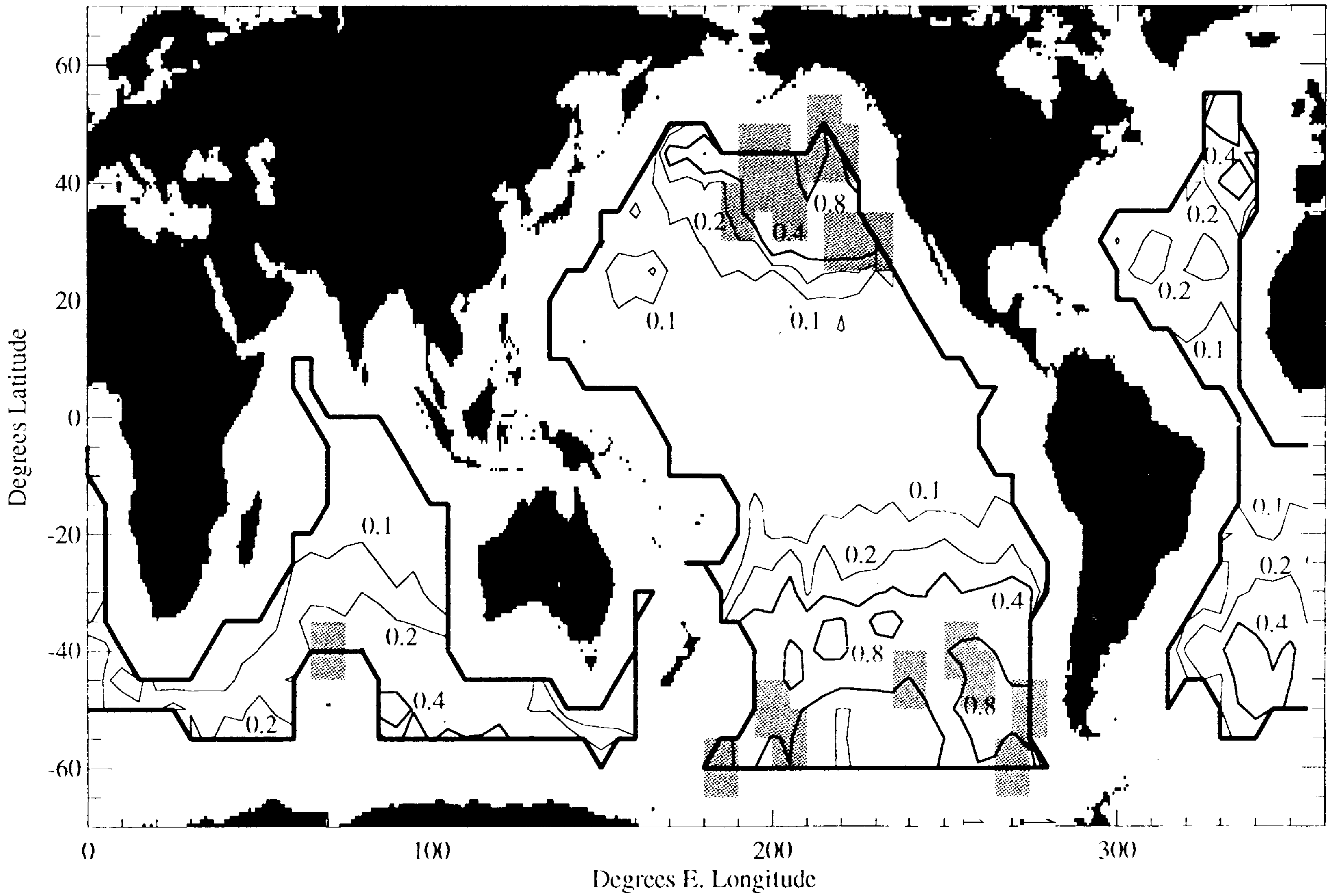
60
40
20
0
-20
-40
-60
Degrees Latitude
0
100
200
300
Degrees E. Longitude
0.1
0.2
0.4
0.8

Fig. 2

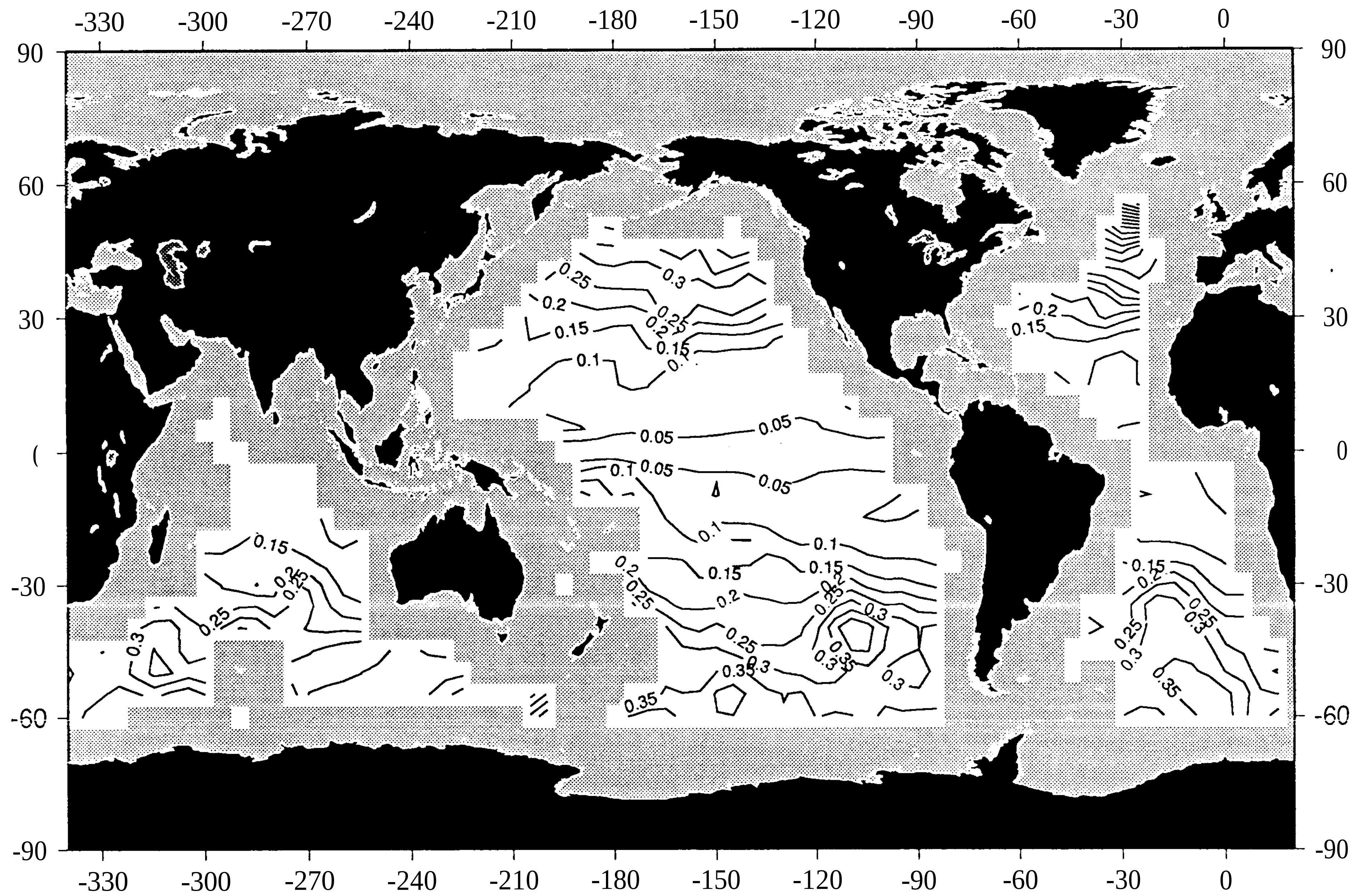
-330 -300 -270 -240 -210 -180 -150 -120 -90 -60 -30 0
90 60 30 0 -30 -60 -90
0.05
0.1
0.15
0.2
0.25
0.3
0.35

Fig 3

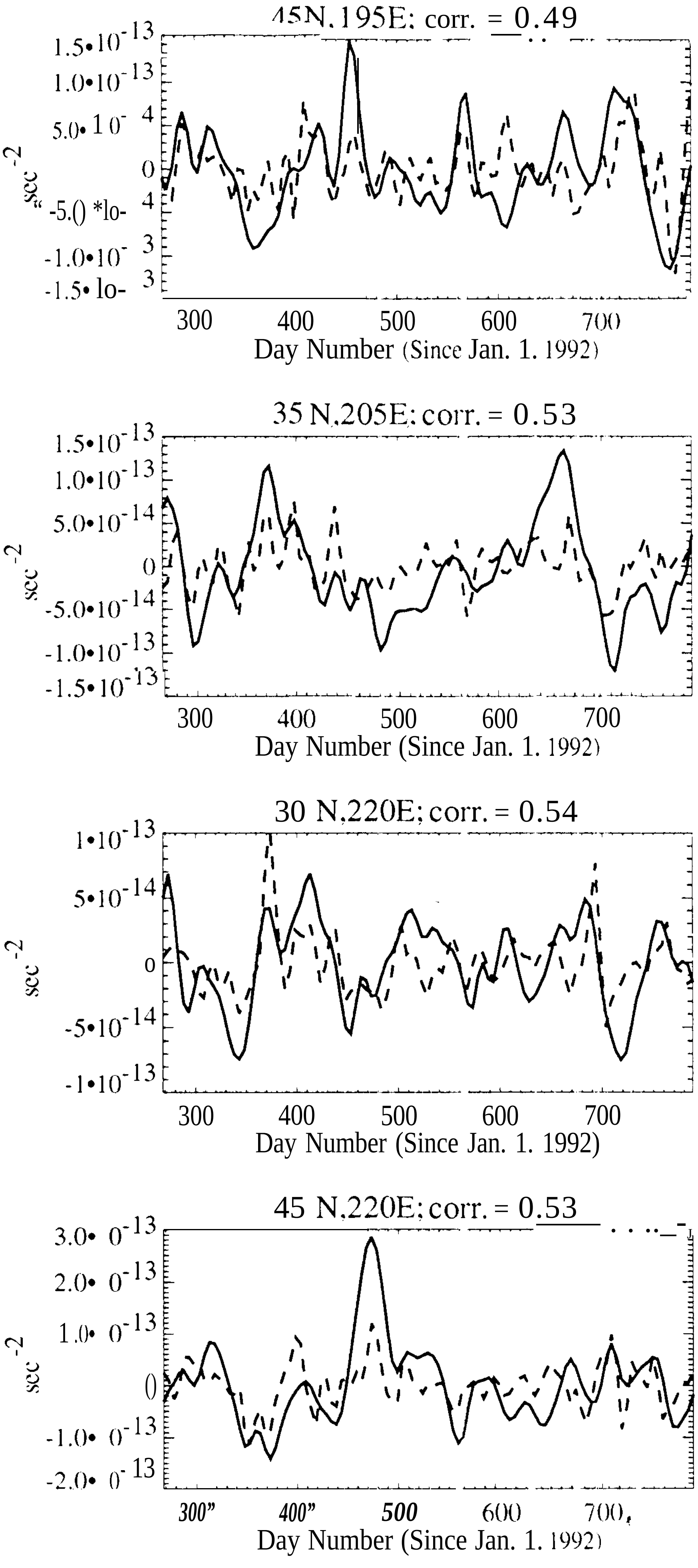
45N,195E; corr. = 0.49
35 N,205E; corr. = 0.53
30 N,220E; corr. = 0.54
45 N,220E; corr. = 0.53
sec^{-2}
Day Number (Since Jan. 1. 1992)
300
400
500
600
700

Fig. 4

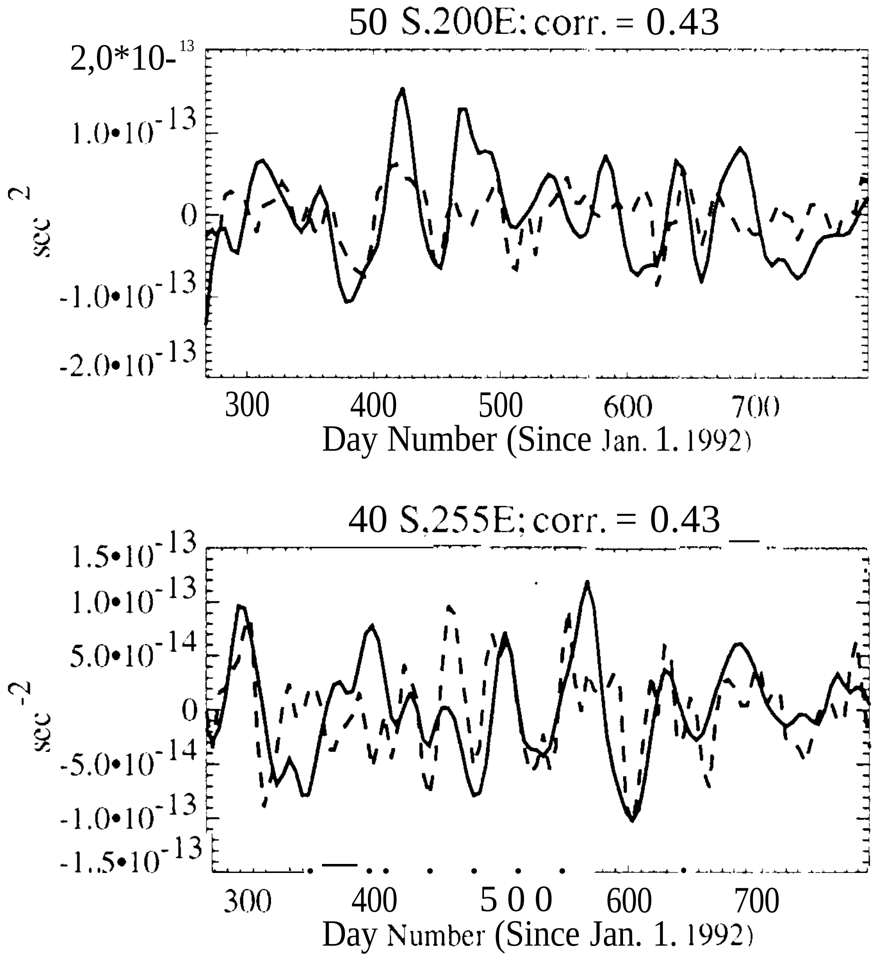
50 S.200E: corr. = 0.43
2,0*10-13
1.0•10-13
0
-1.0•10-13
-2.0•10-13
sec 2
300
400
500
600
700
Day Number (Since Jan. 1. 1992)
40 S,255E; corr. = 0.43
1.5•10-13
1.0•10-13
5.0•10-14
0
-5.0•10-14
-1.0•10-13
-1.5•10-13
sec -2
300
400
500
600
700
Day Number (Since Jan. 1. 1992)

Fig 5

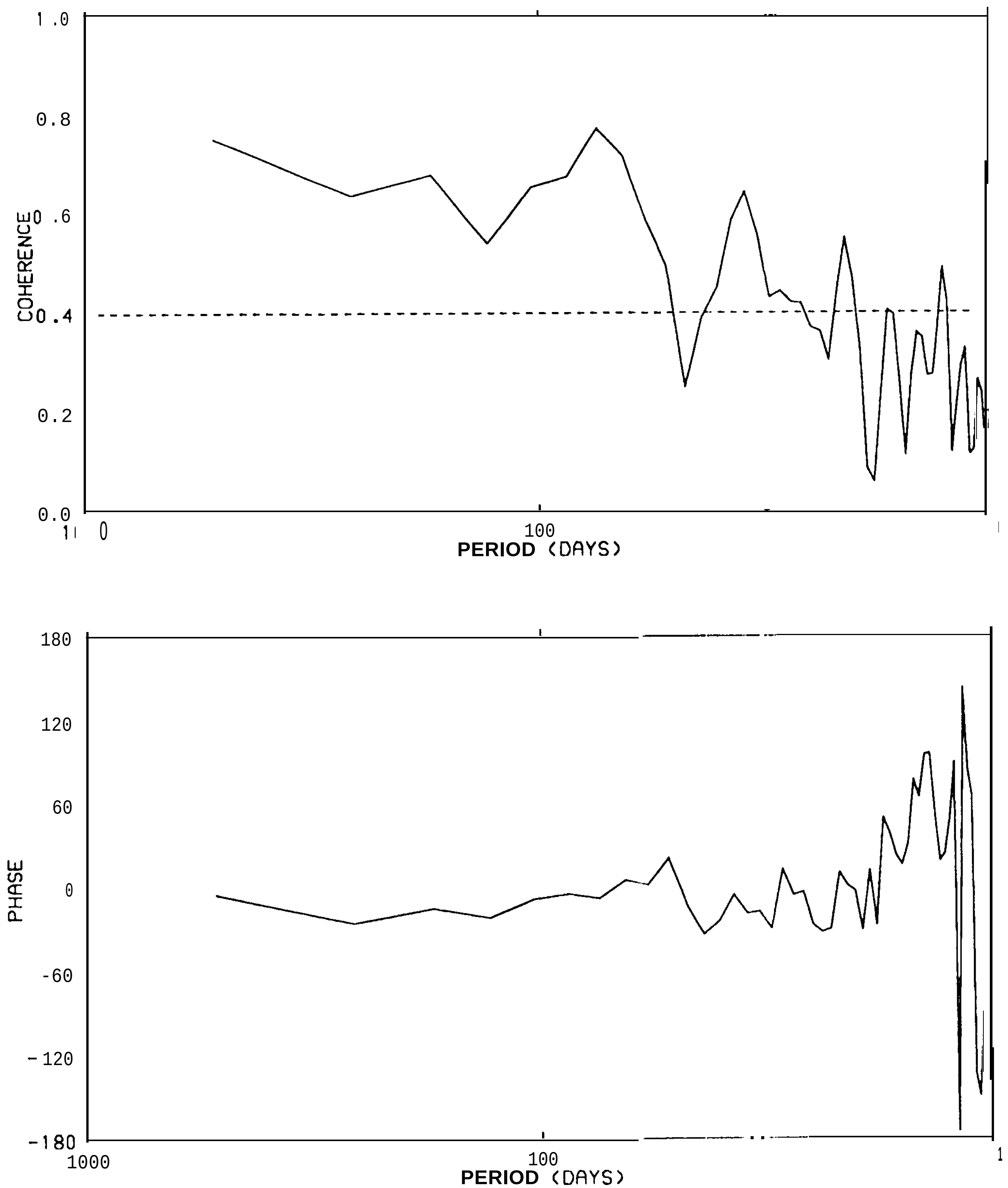
1.0
0.8
0.6
0.4
0.2
0.0
COHERENCE
100
PERIOD (DAYS)
180
120
60
0
-60
-120
-180
PHASE
1000
100
1
PERIOD (DAYS)

Fig. 6

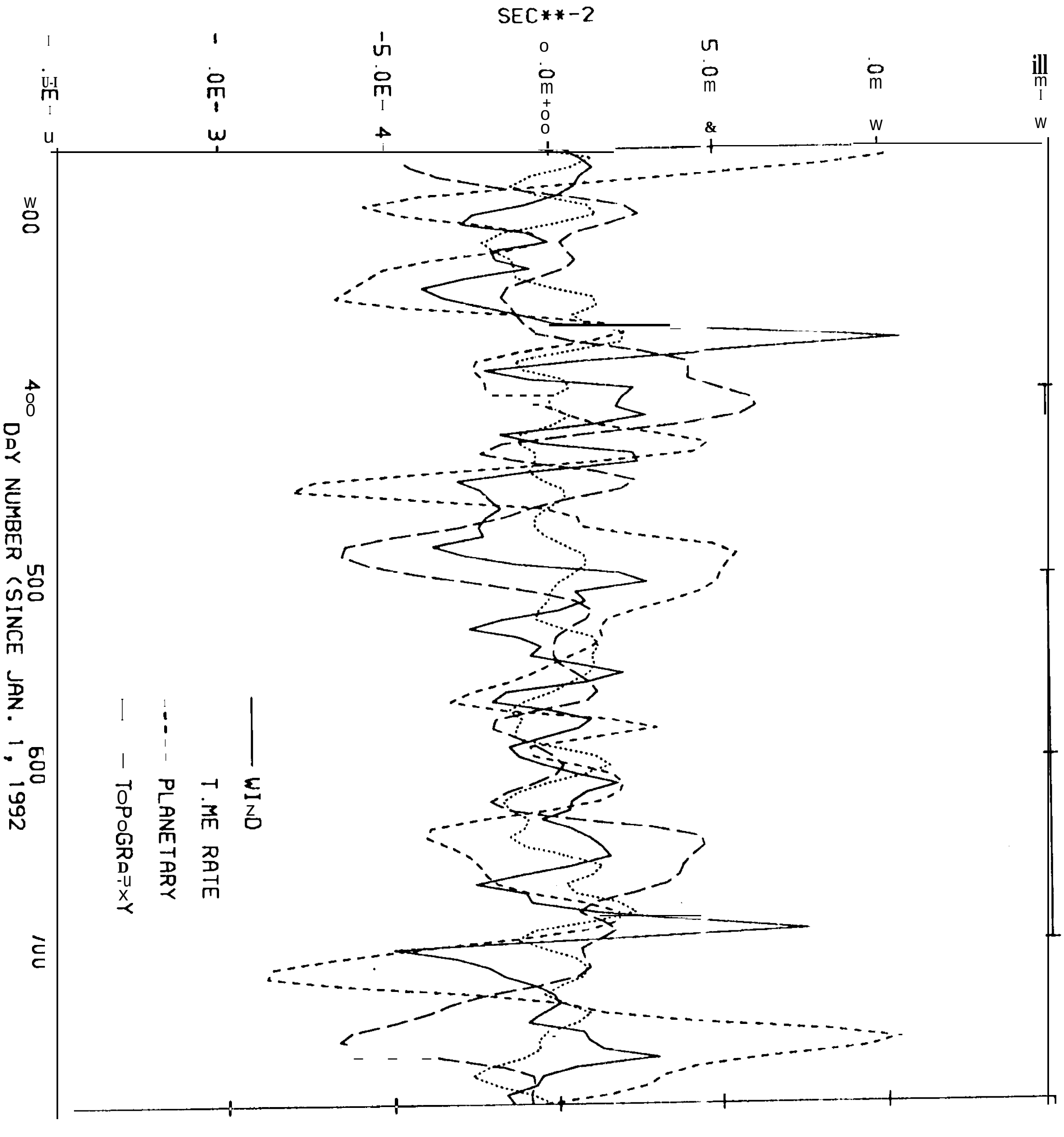
SEC**-2
-5.0E-4
DAY NUMBER (SINCE JAN. 1, 1992
400
500
600
WIND
PLANETARY

Fig. 7a

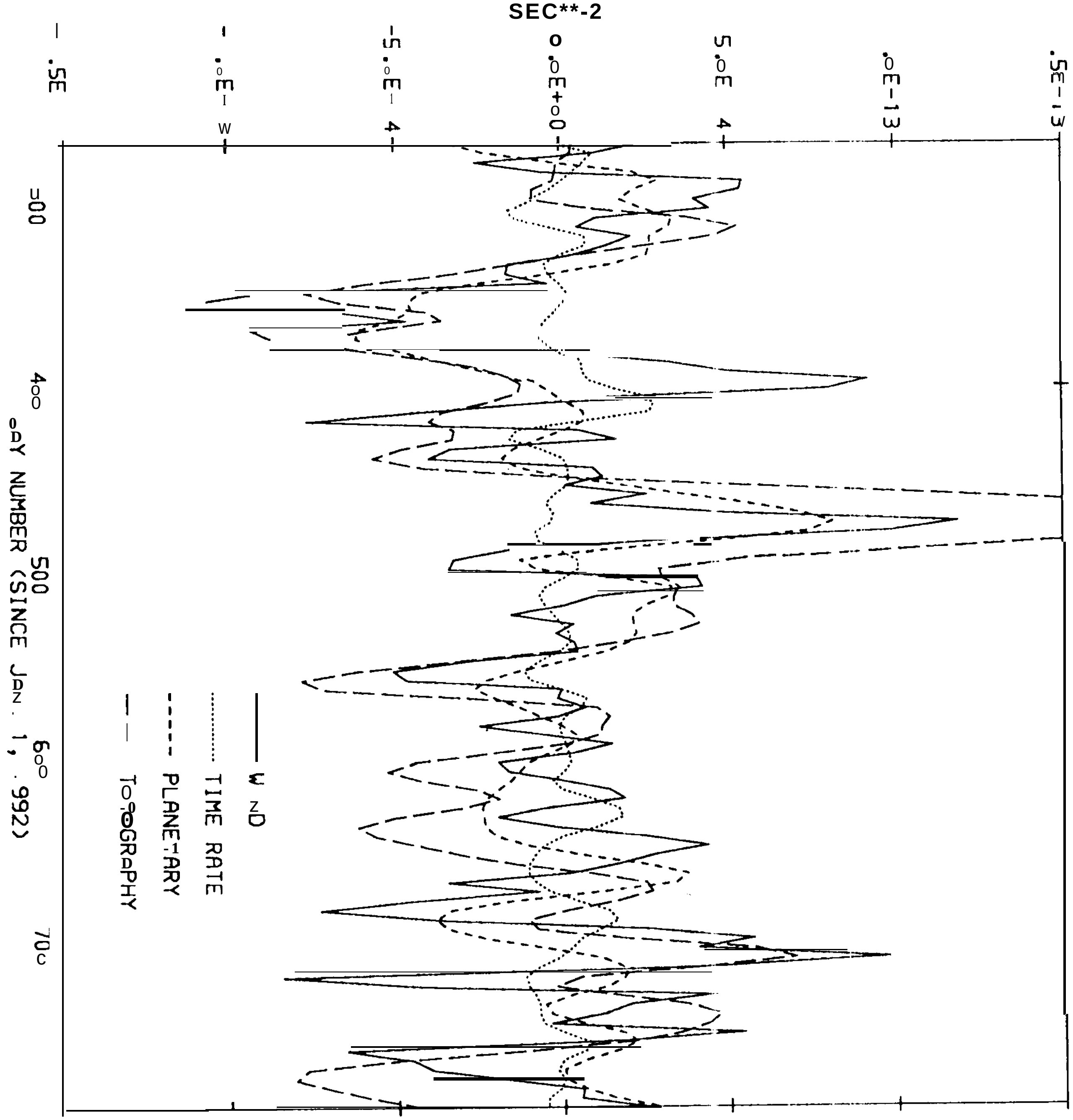

Fig. 7b

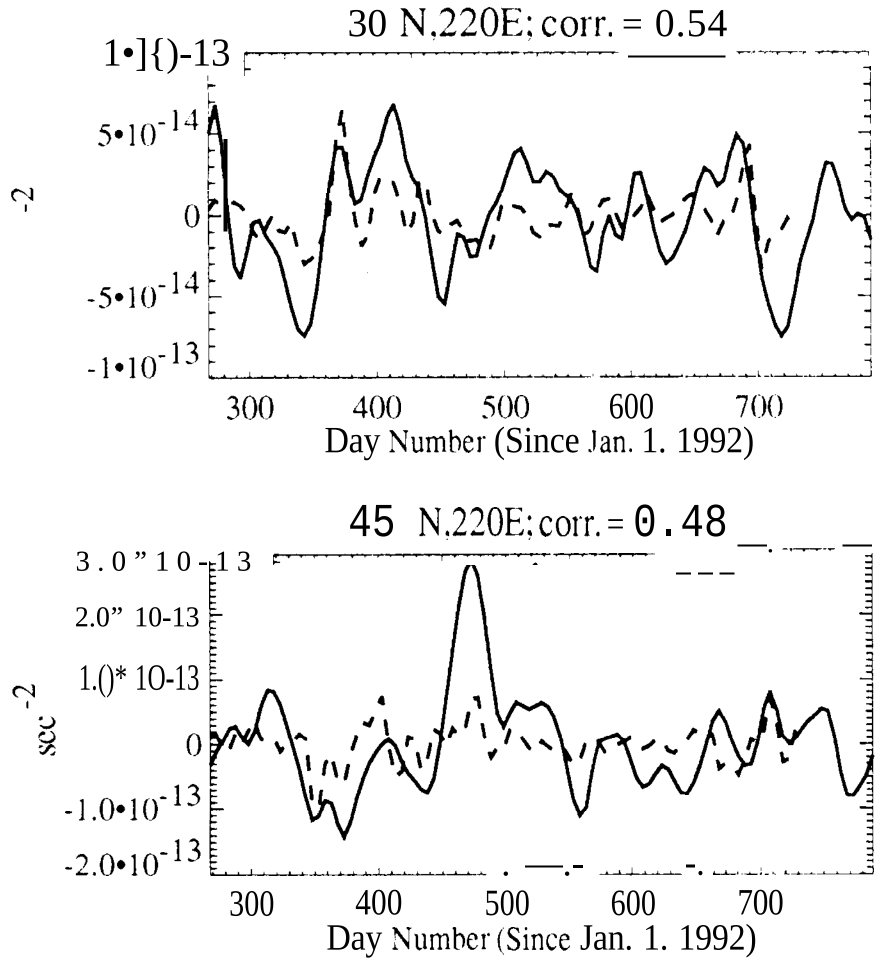
30 N,220E; corr. = 0.54
5•10^-14
0
-5•10^-14
-1•10^-13
-2
300
400
500
600
700
Day Number (Since Jan. 1. 1992)
45 N,220E; corr. = 0.48
3.0•10^-13
2.0•10^-13
1.0•10^-13
0
-1.0•10^-13
-2.0•10^-13
sec^-2
300
400
500
600
700
Day Number (Since Jan. 1. 1992)

Fig. 8